2001-01-1444

Examination of High Frequency Characterization Methods for Mounts

Seungbo Kim and Rajendra Singh
The Ohio State University

ABSTRACT

The knowledge of frequency-dependent dynamic stiffnesses of mounts, in axial and flexural motions, is needed to determine the behavior of many automotive sub-systems. Consequently, characterization and modeling of vibration isolators is increasingly becoming more important in mid and high frequency regimes where very few methods are known to exist. This paper critically examines some of the approximate identification methods that have been proposed in the literature. Then we present a new experimental identification method that yields frequency-dependent multi-dimensional dynamic stiffnesses of an isolator. The scope is however limited to a linear time-invariant system and our analysis is restricted to the frequency domain. The new characterization method uses two inertial elements at both ends of an isolator and free boundary conditions are maintained during testing. Multi-dimensional mobility synthesis formulation is also developed to predict the behavior of overall system, and the decomposed motilities of mount are extracted using synthesized mobilities. The proposed identification method is applied to one simulation example and one practical rubber isolator, and experimental results are successfully compared with data measured on commercial equipment for axial motions.

INTRODUCTION

Experimental methods must be adopted to dynamically characterize stiffnesses of rubber, hydraulic, air and metallic isolators since they invariably exhibit frequency-dependent properties and are sensitive to mean loads and dynamic excitation levels [1-2]. Historically, characterization methods have focused on axial or compressional stiffness since many vibration isolation measures consider only this component [1-6]. However, it has been shown that the rotational stiffness could be a significant contributor to the vibration transmission [7]. Also, in most studies only the lower frequency range has been considered [6-8], and consequently the direct measurement of dynamic stiffness on commercial machines is typically limited to lower frequencies [9].
Several approximate identification methods for transfer stiffness of resilient elements have been proposed for axial (compressional) motions at higher frequencies [10, 11]; these have been further refined for lower frequencies [12, 13]. One such approximate method has also been applied to the identification of flexural stiffnesses [12]. Recently, a new characterization method has also been proposed to examine the nonlinear behavior of isolators at lower frequencies but it is also limited to axial motion [14]. Overall, an appropriate characterization method for the measurement of multi-dimensional stiffnesses of an isolator has yet to be proposed. The underlying measurement and estimation issues are even more difficult as the frequency increases [6, 7]. In this article, we propose a new dynamic characterization method that should be valid over low, mid and high frequency regimes. Further, we introduce a new isolator stiffness matrix formulation. Some subsets of this concept will be examined and compared with existing experimental techniques [10, 11], as well with some recent literature [12, 13]. Problem formulation is conceptually shown in Figure 1.

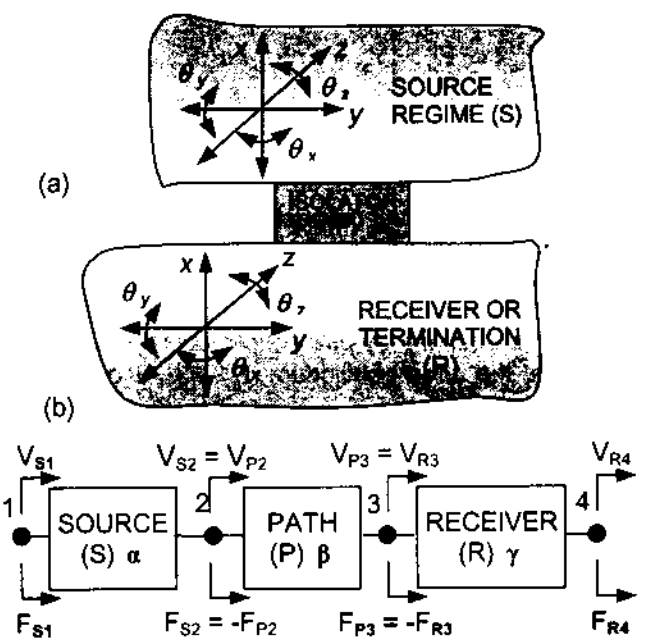

Figure 1. Problem formulation. (a) Isolator is depicted as a multi-dimensional path for any practical problem; (b) source-path-receiver system and their mobility matrices α, β and γ. Here F and V are vectors.

Primary objectives of this study include the following: 1. Propose an analytical framework, based on mobility synthesis method of Figure 1(b) that will synthesize or extract a multi-dimensional stiffness matrix at any given frequency (ω); 2. Suggest a new experimental identification method for spectrally-varying multi-dimensional properties of an isolator (in terms of mobility or stiffness); 3. Apply the proposed identification scheme to one simulation example and one practical isolator example of Figure 2 up to 2 kHz; 4. Examine the methods proposed by Thompson et. al. [10-13] and their underlying assumptions using analytical and numerical methods; and 5. Validate the proposed identification scheme by comparing results with data measured on a commercial machine. The scope is limited to a linear time-invariant (LTI) system, and the effects of preload, etc are not considered.

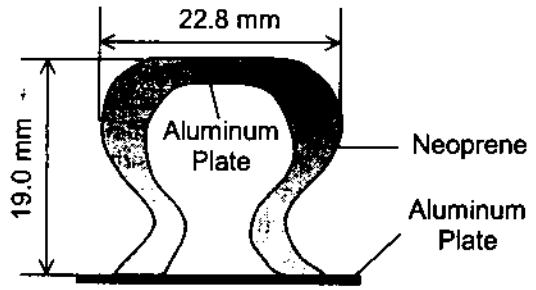

Figure 2. Practical rubber isolator used for experimental studies.

MULTI-DIMENSIONAL MOBILITY SYNTHESIS FORMULATION

SOURCE, PATH AND RECEIVER SYSTEM: Harmonic velocity and interfacial force vectors between sub-systems can be expressed as follows, with reference to Figure 1(b):

$$\mathbf{V}_{S1} = \boldsymbol{\alpha}_{11}\mathbf{F}_{S1} + \boldsymbol{\alpha}_{12}\mathbf{F}_{S2}, \quad \mathbf{V}_{S2} = \boldsymbol{\alpha}_{21}\mathbf{F}_{S1} + \boldsymbol{\alpha}_{22}\mathbf{F}_{S2}, \qquad \text{(1a-b)}$$

$$\mathbf{V}_{P2} = \boldsymbol{\beta}_{22}\mathbf{F}_{P2} + \boldsymbol{\beta}_{23}\mathbf{F}_{P3}, \quad \mathbf{V}_{P3} = \boldsymbol{\beta}_{32}\mathbf{F}_{P2} + \boldsymbol{\beta}_{33}\mathbf{F}_{P3}, \qquad \text{(1c-d)}$$

$$\mathbf{V}_{R3} = \boldsymbol{\gamma}_{33}\mathbf{F}_{R3} + \boldsymbol{\gamma}_{34}\mathbf{F}_{R4}, \quad \mathbf{V}_{R4} = \boldsymbol{\gamma}_{43}\mathbf{F}_{R3} + \boldsymbol{\gamma}_{44}\mathbf{F}_{R4}. \qquad \text{(1e-f)}$$

Here, $\boldsymbol{\alpha}_{ij}$, $\boldsymbol{\beta}_{ij}$ and $\boldsymbol{\gamma}_{ij}$ represent the mobility matrices of source, path and receiver respectively and the ubiquitous (ω) term is dropped for the sake of brevity since only the frequency domain representation is considered. Also, refer to List of symbols for nomenclature. Synthesized formulation is obtained by using the motion compatibility $\mathbf{V}_i = \mathbf{V}_j$ and the force equilibrium $\mathbf{F}_i + \mathbf{F}_j = 0$ conditions at each interface (2 or 3). The mobilities ($\mathbf{M}_{ij}$) of synthesized system are represented in terms of mobilities of components $\boldsymbol{\alpha}_{ij}$, $\boldsymbol{\beta}_{ij}$ and $\boldsymbol{\gamma}_{ij}$. Details may be found in reference [15].

DECOMPOSITION OF COMPONENT MOBILITIES: Let us assume that an isolator acts as a path in Figure 1(b). Its mobility $\boldsymbol{\beta}_{ij}$ for i, j = 2, 3 is defined where $\mathbf{V}_{P2} = \boldsymbol{\beta}_{22}\mathbf{F}_{P2}$, $\mathbf{V}_{P2} = \boldsymbol{\beta}_{23}\mathbf{F}_{P3}$, $\mathbf{V}_{P3} = \boldsymbol{\beta}_{32}\mathbf{F}_{P2}$ and $\mathbf{V}_{P3} = \boldsymbol{\beta}_{33}\mathbf{F}_{P3}$. Therefore, we need to extract four unknowns $\boldsymbol{\beta}_{22}$, $\boldsymbol{\beta}_{23}$, $\boldsymbol{\beta}_{32}$ and $\boldsymbol{\beta}_{33}$ from the mobilities of the combined system. Details are given in reference [15].

SIMULATION EXAMPLE FOR MOBILITY SYNTHESIS AND DECOMPOSITION

Figure 3(b) shows a simulation example that consists of an elastic beam and two rigid masses where EI_s is the flexural rigidity of beam and I_m is the moment of inertia corresponding to lumped masses (m_a and m_b). Here, f and q are harmonic force and moment excitation amplitudes respectively at frequency ω, and subscripts a, b and G represent mass a, mass b and mass center respectively. Mobilities of the combined system are obtained from the mobility synthesis formulation and compared with the direct analytical solution.

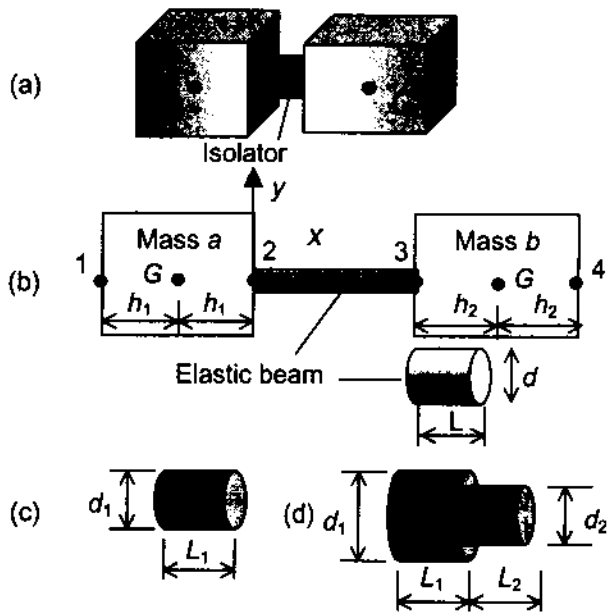

Figure 3. Proposed identification scheme. (a) Schematic; (b) simulation example; (c) symmetric isolator used for simulation; (d) asymmetric isolator used for simulation.

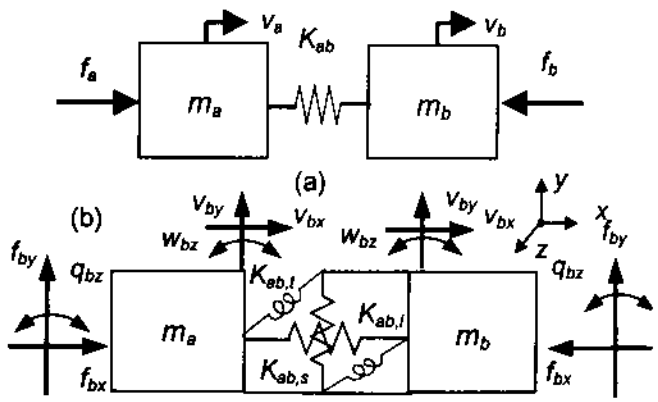

Figure 4. Lumped approximations of system of Figure 3(a). (a) Isolator is modeled via a scalar stiffness in axial direction; (b) isolator is described by multi-dimensional stiffness terms. Here $K_{ab,l}$, $K_{ab,s}$ and $K_{ab,t}$ represent axial, shear and rotational stiffnesses respectively.

MOBILITY MATRIX OF A RIGID BODY: Assume that the source of Figure 1(a) is a rigid body like the example of Figure 3(a). Now we determine the mobility matrix that

characterizes the relationship between multi-dimensional excitations at frequency ω and the steady state velocity responses through the rigid mass (m). First, the mobility matrix $\mathbf{M}$ (ω) is defined in terms of velocity vector $\mathbf{V}_G$ at the mass center (G), $\mathbf{V}_G = \mathbf{M}_{GG}\mathbf{F}_G$ where $\mathbf{F}_G$ is excitation vector. Decompose the formulation in terms of translational (**v**) and rotational (**w**) components, and define

$$\mathbf{M}_{GG} = \begin{bmatrix} \mathbf{M}_{v,GG} & 0 \\ 0 & \mathbf{M}_{w,GG} \end{bmatrix}, \quad (2a)$$

$$\mathbf{M}_{v,GG} = diag\left(\begin{bmatrix} \frac{1}{mj\omega} & \frac{1}{mj\omega} & \frac{1}{mj\omega} \end{bmatrix} \right), \quad (2b)$$

$$\mathbf{M}_{w,GG} = \frac{1}{j\omega} \begin{bmatrix} I_{m,xx} & -I_{m,xy} & -I_{m,xz} \\ -I_{m,xy} & I_{m,yy} & -I_{m,yz} \\ -I_{m,xz} & -I_{m,yz} & I_{m,zz} \end{bmatrix}^{-1}, \quad (2c)$$

$$\mathbf{V}_G = \begin{bmatrix} \mathbf{v}_G \\ \mathbf{w}_G \end{bmatrix}, \qquad \mathbf{F}_G = \begin{bmatrix} \mathbf{f}_G \\ \mathbf{q}_G \end{bmatrix}. \quad (2d\text{-}e)$$

The mobility matrix of a rigid body, between any two points i and j, can be determined as follows:

$$\begin{bmatrix} \mathbf{V}_i \\ \mathbf{V}_j \end{bmatrix} = \begin{bmatrix} \mathbf{M}_{ii} & \mathbf{M}_{ij} \\ \mathbf{M}_{ji} & \mathbf{M}_{jj} \end{bmatrix} \begin{bmatrix} \mathbf{F}_i \\ \mathbf{F}_j \end{bmatrix} = \begin{bmatrix} \mathbf{T}_i^T \mathbf{M}_{GG} \mathbf{T}_i & \mathbf{T}_i^T \mathbf{M}_{GG} \mathbf{T}_j \\ \mathbf{T}_j^T \mathbf{M}_{GG} \mathbf{T}_i & \mathbf{T}_j^T \mathbf{M}_{GG} \mathbf{T}_j \end{bmatrix} \begin{bmatrix} \mathbf{F}_i \\ \mathbf{F}_j \end{bmatrix}. \quad (3)$$

where

$$\mathbf{T}_i = \begin{bmatrix} \mathbf{I} & 0 \\ \mathbf{R}_i & \mathbf{I} \end{bmatrix}, \quad \mathbf{R}_i = \begin{bmatrix} 0 & -h_{zi} & h_{yi} \\ h_{zi} & 0 & -h_{xi} \\ -h_{yi} & h_{xi} & 0 \end{bmatrix}. \quad (4a\text{-}b)$$

COMPARISON OF TWO METHODS: Calculations are performed using both procedures for a circular beam with modulus of elasticity (E) of 8 x 10^5 N/m^2, mass density (ρ) of 1000 kg/m^3 and a loss factor (η) of 0.1. The radius and length of the beam are 12 mm and 30 mm respectively. Masses of rigid bodies *a* and *b* are 0.65 kg and 0.55 kg respectively, and the corresponding dimensions in x, y and z directions are 75 mm, 50 mm and 64 mm for mass *a* and 68 mm, 50 mm and 50 mm for mass *b*. Mobilities of the combined system are calculated by employing the mobility synthesis formulation based on the base driven beam mobilities and the mobilities of rigid bodies *a* and *b*.

Predictions via the mobility synthesis formulation compare well with the direct analytical solution, though not shown here. Also, the mobilities of beam are extracted from the results of the combined system and then compared with the analytical mobilities of beam. As evident from the results of Figures 5 and 6, both methods yield the same answers. Only the proposed mobility method will be used in further studies.

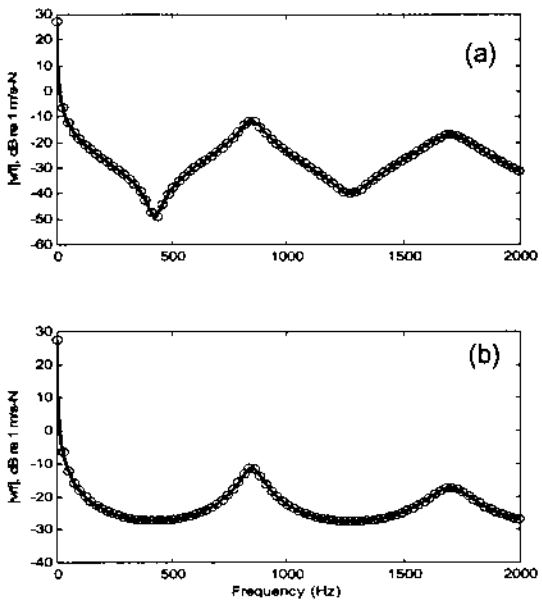

Figure 5. Decomposed mobilities for beam using a system consisting of two rigid masses and an elastic beam as shown in Figure 3(b). (a) Driving point mobility; (d) transfer mobility. Key: ——— , Decomposed mobility; o, direct analytical solution.

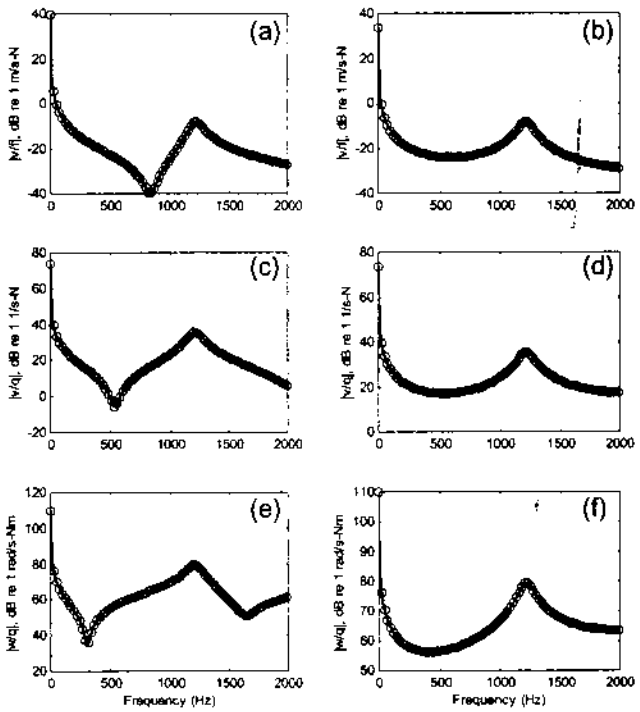

Figure 6. Decomposed mobilities for beam using a system consisting of two rigid masses and an elastic beam as shown in Figure 3(b). (a) Driving point force mobility; (b) driving point coupling mobility; (c) driving point moment mobility; (d) transfer force mobility; (e) transfer coupling mobility; (f) transfer moment mobility. Key: ——— , Decomposed mobility; o, direct analytical solution.

EXAMINATION OF APPROXIMATE METHODS

Several attempts have been made for the identification of transfer stiffnesses including the rotational component [10-13]. Such schemes typically consider a resilient element that is located between two inertial components as shown in Figure 7. The first method focuses on high frequency properties [10-11] and it may be applied to either axial or flexural motions. And, the second method improves the axial (compressional) stiffness at low frequencies by modifying the first scheme [12-13]. In our study, key procedures of such approximate methods are briefly explained, using the mobility method for the sake of consistency. Both approximate schemes are analytically examined using a simulation example. Further, the second approximate method is extended to the identification of flexural stiffnesses.

APPROXIMATE METHOD FOR AXIAL MOTIONS: The discrete system of Figure 7 is examined using the mobility method. This obviously yields the results reported by Thompson et. al. [12] based on lumped system theory. Here, β_{22} and β_{33} are the driving point mobilities of isolator, β_{23} and β_{32} are the transfer mobilities of isolator. Note that K_{11}, K_{22}, K_{12} and K_{21} are the corresponding axial stiffnesses of the isolator. And, K_1 and K_2 are the stiffnesses of additional elastic elements attached to rigid masses *a* and *b* respectively for experimental purposes. Further, f_2 and f_3 are interfacial forces at connecting locations.

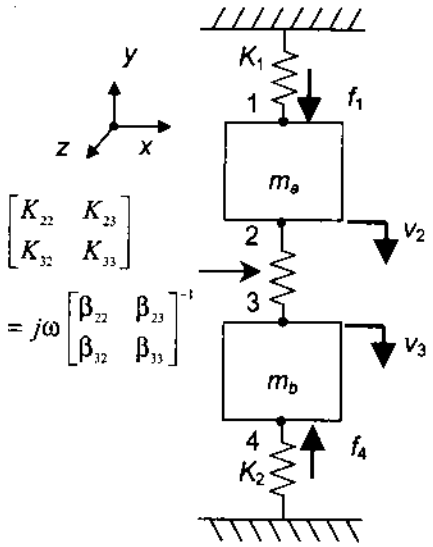

Figure 7. Discrete model of physical system used to examine approximate methods.

The governing equations are

$$[\, j\omega m_a + K_1/j\omega \,]\, v_2 = -f_2 + f_1 , \qquad (5a)$$

$$[\, j\omega m_b + K_2/j\omega \,]\, v_3 = -f_3 , \qquad (5b)$$

$$[\, j\omega m_a + K_1/j\omega \,]\, v_2 = -f_2 , \qquad (5c)$$

$$[\, j\omega m_b + K_2/j\omega \,]\, v_3 = -f_3 + f_4 , \qquad (5d)$$

$$v_2 = \beta_{22} f_2 + \beta_{23} f_3 , \quad v_3 = \beta_{32} f_2 + \beta_{33} f_3 . \qquad (5e\text{-}f)$$

Using (5a-f) and eliminating interfacial forces, the following equations are obtained when an external force (f_1) is applied at rigid mass *a*:

$$\beta_{22}[\, j\omega m_a + K_1/j\omega + 1/\beta_{22} \,]\, v_2 + \beta_{23}[\, j\omega m_b + K_2/j\omega \,]\, v_3 = \beta_{22} , \qquad (6a)$$

$$\beta_{32}[\, j\omega m_a + K_1/j\omega \,]\, v_2 + \beta_{33}[\, j\omega m_b + K_2/j\omega + 1/\beta_{33} \,]\, v_3 = \beta_{32} . \qquad (6b)$$

Simultaneous solution of (6a-b) yields the driving point and transfer mobilities:

$$M_{11} = v_1/f_1 = \frac{[j\omega m_b + K_2/j\omega][\beta_{22}\beta_{33} - \beta_{23}\beta_{32}] + \beta_{22}}{\Delta(\omega)} , \qquad (7a)$$

$$M_{41} = v_4/f_1 = \frac{\beta_{32}}{\Delta(\omega)} , \qquad (7b)$$

where

$$\Delta(\omega) = (j\omega m_a + K_1/j\omega)\beta_{22} + (j\omega m_b + K_2/j\omega)\beta_{22} + (j\omega m_a + K_1/j\omega)(j\omega m_b + K_2/j\omega)[\beta_{22}\beta_{33} - \beta_{23}\beta_{32}] + 1 . \qquad (7c)$$

In a similar manner, governing equations and mobilities are written as follows when an external force (f_4) is applied at rigid mass *b*:

$$\beta_{22}[\, j\omega m_a + K_1/j\omega + 1/\beta_{22} \,]\, v_2 + \beta_{23}[\, j\omega m_b + K_2/j\omega \,]\, v_3 = \beta_{23} , \qquad (8a)$$

$$\beta_{32}[\, j\omega m_a + K_1/j\omega \,]\, v_2 + \beta_{33}[\, j\omega m_b + K_2/j\omega + 1/\beta_{33} \,]\, v_3 = \beta_{33} , \qquad (8b)$$

$$M_{14} = v_1/f_4 = \frac{\beta_{23}}{\Delta(\omega)} , \qquad (9a)$$

$$M_{44} = v_4/f_4 = \frac{[j\omega m_a + K_1/j\omega][\beta_{22}\beta_{33} - \beta_{23}\beta_{32}] + \beta_{33}}{\Delta(\omega)} . \qquad (10b)$$

From (7a-b), the motion transmissibility between two rigid masses is

$$\frac{v_4}{v_1} = \frac{\beta_{32}}{[j\omega m_b + K_2/j\omega][\beta_{22}\beta_{33} - \beta_{23}\beta_{32}] + \beta_{22}} = \frac{-K_{32}}{K_2 + K_{33} - m_b\omega^2} . \qquad (11)$$

From the above transmissibility, transfer stiffness of an isolator K_{32} is extracted by assuming that $(K_2 + K_{33}) << \omega^2 m_b$ at high frequencies such that $\omega > \omega'$ where $\omega' = 3\sqrt{(K_2 + K_{33})/m_b}$, as reported by Thompson et. al. [12]:

$$K_{32} \approx (-\omega^2 m_b)\frac{v_4}{v_1} \qquad \text{for } \omega > \omega' . \qquad (12)$$

This approximate method provides reasonable results for transfer stiffness at higher frequencies, but yields a poor estimation at lower frequencies ($\omega > \omega'$). In order to enhance the identification scheme at low frequencies, the following transfer function is introduced in place of the typical motion transmissibility term [12]:

$$\frac{v_4}{v_1 - v_4} = \frac{\beta_{32}}{[j\omega m_b + K_2/j\omega][\beta_{22}\beta_{33} - \beta_{23}\beta_{32}] + \beta_{22} + \beta_{32}} = \frac{-K_{32}}{K_2 - m_b\omega^2 + K_{33} - K_{32}} . \qquad (13)$$

From the above transfer function, the transfer stiffness is now approximated as follows by assuming

that it is equal to the driving point stiffness where $\omega^* = \sqrt{K_2/m_b}$ [12]:

$$K_{32} \approx (-\omega^2 m_b)\frac{v_4}{v_3 - v_4} \qquad \text{for } \omega > \omega^*. \qquad (14)$$

APPROXIMATE METHOD FOR FLEXURAL MOTIONS: Unlike the analysis of Thompson et. al. [12], now we examine this system in flexural motions. Again, we employ the mobility method where β_{22} and β_{33} are the driving point mobilities of isolator, β_{23} and β_{32} are the transfer mobilities of isolator in flexure. Further, K_{11}, K_{22}, K_{12} and K_{21} are corresponding flexural stiffnesses of the isolator. And, K_1 and K_2 are the flexural stiffnesses of additional elastic elements. Subscripts $x\theta$ and θx represent coupling mobilities or stiffnesses, and xx and $\theta\theta$ are used for diagonal terms. For rigid masses, h is the distance between mass center and connecting locations of the isolator and I_G is the mass moment of inertia with respect to its mass center. Here f_2 and f_3 are interfacial forces and moments at connections, and f_{2e} and f_{3e} are external forces and q_{2e} and q_{3e} are external moments. The governing equations are

$$j\omega m_a v_{1Gx} + [K_{1,xx}v_{1x} + K_{1,x\theta}w_1]/j\omega = -f_{2x} + f_{2xe}, \qquad (15a)$$

$$[j\omega I_{aG} w_1 - j\omega m_a h_a v_{1Gx}] + [-(K_{1,xx}v_{1x} + K_{1,x\theta}w_1)2h_a + K_{1,\theta x}v_{1x} + K_{1,\theta\theta}w_1]/j\omega = -q_2 + q_{2e}, \qquad (15b)$$

$$j\omega m_b v_{2Gx} + [K_{2,xx}v_{4x} + K_{2,x\theta}w_4]/j\omega = -f_{3x}, \qquad (15c)$$

$$[j\omega I_{bG} w_1 - j\omega m_b h_b v_{2Gx}] + [-(K_{2,xx}v_{4x} + K_{2,x\theta}w_4)2h_b + K_{2,\theta x}v_{4x} + K_{2,\theta\theta}w_4]/j\omega = -q_3, \qquad (15d)$$

$$v_{2x} = \beta_{22,xx}f_{2x} + \beta_{22,x\theta}q_2 + \beta_{23,xx}f_{3x} + \beta_{23,x\theta}q_3, \qquad (15e)$$

$$w_2 = \beta_{22,\theta x}f_{2x} + \beta_{22,\theta\theta}q_2 + \beta_{23,\theta x}f_{3x} + \beta_{23,\theta\theta}q_3, \qquad (15f)$$

$$v_{3x} = \beta_{32,xx}f_{2x} + \beta_{32,x\theta}q_2 + \beta_{33,xx}f_{3x} + \beta_{33,x\theta}q_3, \qquad (15g)$$

$$w_3 = \beta_{32,\theta x}f_{2x} + \beta_{32,\theta\theta}q_2 + \beta_{33,\theta x}f_{3x} + \beta_{33,\theta\theta}q_3. \qquad (15h)$$

Represent the above equations of motion in matrix form as follows:

$$[j\omega\mathbf{m}_a + \frac{1}{j\omega}\mathbf{K}_1]\,\mathbf{V}_2 = -\mathbf{F}_2 + \mathbf{F}_{2e}, \qquad (16a)$$

$$[j\omega\mathbf{m}_b + \frac{1}{j\omega}\mathbf{K}_2]\,\mathbf{V}_3 = -\mathbf{F}_3, \qquad (16b)$$

$$\mathbf{V}_2 = \boldsymbol{\beta}_{22}\mathbf{F}_2 + \boldsymbol{\beta}_{23}\mathbf{F}_3, \qquad (16c)$$

$$\mathbf{V}_3 = \boldsymbol{\beta}_{32}\mathbf{F}_2 + \boldsymbol{\beta}_{33}\mathbf{F}_3, \qquad (16d)$$

where

$$\mathbf{m}_a = \begin{bmatrix} m_a & -m_a h_a \\ -m_a h_a & I_{aG} + m_a h_a^2 \end{bmatrix}, \qquad (16e)$$

$$\mathbf{m}_b = \begin{bmatrix} m_b & m_b h_b \\ m_b h_b & I_{bG} + m_b h_b^2 \end{bmatrix}, \qquad (16f)$$

$$\mathbf{K}_1 = \frac{1}{j\omega}\begin{bmatrix} K_{1,xx} & -2h_a K_{1,xx} + K_{1,x\theta} \\ -2h_a K_{1,xx} + K_{1,\theta x} & 4h_a^2 K_{1,xx} - 2h_a(K_{1,x\theta} + K_{1,\theta x}) + K_{1,\theta\theta} \end{bmatrix}, \qquad (16g)$$

$$\mathbf{K}_2 = \frac{1}{j\omega}\begin{bmatrix} K_{2,xx} & 2h_b K_{2,xx} + K_{2,x\theta} \\ 2h_b K_{2,xx} + K_{2,\theta x} & 4h_b^2 K_{2,xx} + 2h_b(K_{2,x\theta} + K_{2,\theta x}) + K_{2,\theta\theta} \end{bmatrix}, \qquad (16h)$$

$$\boldsymbol{\beta}_{22} = \begin{bmatrix} \beta_{22,xx} & \beta_{22,x\theta} \\ \beta_{22,\theta x} & \beta_{22,\theta\theta} \end{bmatrix}, \qquad \boldsymbol{\beta}_{23} = \begin{bmatrix} \beta_{23,xx} & \beta_{23,x\theta} \\ \beta_{23,\theta x} & \beta_{23,\theta\theta} \end{bmatrix}, \qquad (16i\text{-}j)$$

$$\boldsymbol{\beta}_{32} = \begin{bmatrix} \beta_{32,xx} & \beta_{32,x\theta} \\ \beta_{32,\theta x} & \beta_{32,\theta\theta} \end{bmatrix}, \qquad \boldsymbol{\beta}_{33} = \begin{bmatrix} \beta_{33,xx} & \beta_{33,x\theta} \\ \beta_{33,\theta x} & \beta_{33,\theta\theta} \end{bmatrix}, \qquad (16k\text{-}l)$$

$$\mathbf{F}_2 = [f_2 \quad q_2]; \quad \mathbf{F}_3 = [f_3 \quad q_3]; \quad \mathbf{F}_{2e} = [f_{2e} \quad q_{2e}]. \qquad (16m\text{-}o)$$

Similar to the axial case, interfacial forces are eliminated from (16a-d), and equations of motion are rewritten as follows:

$$[j\omega\mathbf{m}_a + \frac{1}{j\omega}\mathbf{K}_1 + \boldsymbol{\beta}_{22}^{-1}]\,\mathbf{V}_2 + \boldsymbol{\beta}_{22}^{-1}\boldsymbol{\beta}_{23}[j\omega\mathbf{m}_b + \frac{1}{j\omega}\mathbf{K}_2]\,\mathbf{V}_3 = \mathbf{F}_{2e}, \qquad (17a)$$

$$[j\omega\mathbf{m}_a + \frac{1}{j\omega}\mathbf{K}_1]\,\mathbf{V}_2 + \boldsymbol{\beta}_{32}^{-1}\boldsymbol{\beta}_{33}[j\omega\mathbf{m}_b + \frac{1}{j\omega}\mathbf{K}_2 + \boldsymbol{\beta}_{33}^{-1}]\,\mathbf{V}_3 = \mathbf{F}_{2e}. \qquad (17b)$$

Finally, the motion transmissibility in flexural motion is obtained as follows using (17):

$$[\,[\,\boldsymbol{\beta}_{33} - \boldsymbol{\beta}_{32}\boldsymbol{\beta}_{22}^{-1}\boldsymbol{\beta}_{23}]^{-1} + [\,j\omega\mathbf{m}_b + \frac{1}{j\omega}\mathbf{K}_2\,]\,]^{-1} \cdot [\,\boldsymbol{\beta}_{22}\boldsymbol{\beta}_{32}^{-1}\boldsymbol{\beta}_{33} - \boldsymbol{\beta}_{23}]^{-1}\,\mathbf{V}_2 = \mathbf{V}_3 \qquad (18)$$

Next, the stiffness matrix can be partitioned and represented by sub-matrices of the mobility matrix by using the following:

$$\mathbf{K} = \begin{bmatrix} \mathbf{K}_{22} & \mathbf{K}_{23} \\ \mathbf{K}_{32} & \mathbf{K}_{33} \end{bmatrix} = j\omega\boldsymbol{\beta}^{-1} = j\omega\begin{bmatrix} \boldsymbol{\beta}_{22} & \boldsymbol{\beta}_{23} \\ \boldsymbol{\beta}_{32} & \boldsymbol{\beta}_{33} \end{bmatrix}^{-1} \downarrow = j\omega\begin{bmatrix} [\,\boldsymbol{\beta}_{22} - \boldsymbol{\beta}_{23}\boldsymbol{\beta}_{33}^{-1}\boldsymbol{\beta}_{32}]^{-1} & -[\,\boldsymbol{\beta}_{33}\boldsymbol{\beta}_{23}^{-1}\boldsymbol{\beta}_{22} - \boldsymbol{\beta}_{32}]^{-1} \\ -[\,\boldsymbol{\beta}_{22}\boldsymbol{\beta}_{32}^{-1}\boldsymbol{\beta}_{33} - \boldsymbol{\beta}_{23}]^{-1} & [\,\boldsymbol{\beta}_{33} - \boldsymbol{\beta}_{32}\boldsymbol{\beta}_{22}^{-1}\boldsymbol{\beta}_{23}]^{-1} \end{bmatrix} \qquad (19)$$

Using (19), the motion transmissibility can be represented in terms of stiffness matrices as follows:

$$-[\,\mathbf{K}_2 - \omega^2\mathbf{m}_b + \mathbf{K}_{33}]^{-1}\,\mathbf{K}_{32}\,\mathbf{V}_2 = \mathbf{V}_3. \qquad (20a)$$

Therefore, the transfer stiffness matrix of an isolator is approximated as follows where $(\mathbf{V}_3 \,|\, \mathbf{V}_2)$ represents the velocity transmissibility between rigid masses a and b where | represents a complex quotient operation for matrices:

$$\mathbf{K}_{32} \approx \omega^2\mathbf{m}_b\,(\mathbf{V}_3 \,|\, \mathbf{V}_2). \qquad (20b)$$

Similarly, the transfer function matrix between $[\mathbf{V}_2 - \mathbf{V}_3]$ and $\mathbf{V}_3$ can be defined as follows:

$$-[\,\mathbf{K}_2 - \omega^2\mathbf{m}_b + \mathbf{K}_{33} + \mathbf{K}_{32}]^{-1}\,\mathbf{K}_{32}\,(\mathbf{V}_2 - \mathbf{V}_3) = \mathbf{V}_3. \qquad (21a)$$

Analogous to the identification of axial stiffness, the transfer stiffness matrix of isolator in flexure is approximated from (21a) as follows where $[\mathbf{V}_3 \,|\, (\mathbf{V}_2 - \mathbf{V}_3)]$ represents the transfer function matrix that is defined by (21a):

$$\mathbf{K}_{32} \approx \omega^2\mathbf{m}_b\,[\mathbf{V}_3 \,|\, (\mathbf{V}_2 - \mathbf{V}_3)]. \qquad (21b)$$

SIMULATION EXAMPLE: In order to critically examine the generality of the original and refined schemes by Thompson et. al. [12], a simulation example is chosen and symmetric and asymmetric isolators as shown in

Figure 3(c, d) are examined. Simulation results are shown in Figure 8 for axial stiffness and Figures 9 and 10 for flexural stiffnesses.

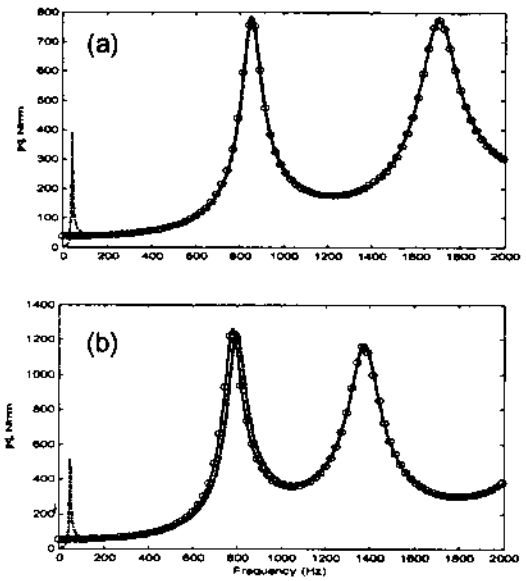

Figure 8. Decomposed axial stiffness for beam using a system consisting of two rigid masses and an elastic beam as shown in Figure 3(b). (a) Symmetric beam of Figure 3(c); (b) asymmetric beam of Figure 3(d). Key: ——, Mobility synthesis method; –·–·– , approximate method using equation (12); _____ , approximate method using equation (14); o, direct analytical solution.

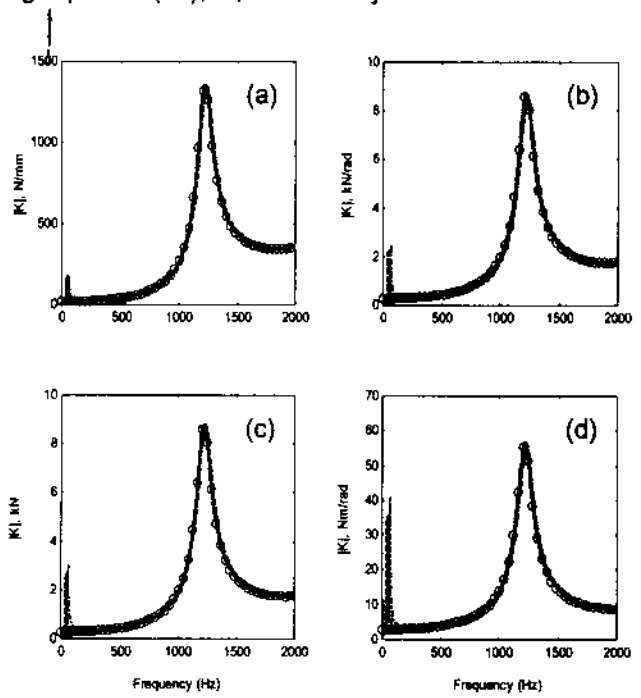

Figure 9. Decomposed flexural stiffnesses for symmetric beam of Figure 3(c) using a system consisting of two rigid masses and an elastic beam as shown in Figure 3(b). (a) Force stiffness; (b) coupling stiffness; (c) coupling stiffness; (d) moment stiffness. Key: —— , Mobility synthesis method; _·_·_ , approximate method using equation (20b); ----- , approximate method using equation (21b); o, direct analytical solution.

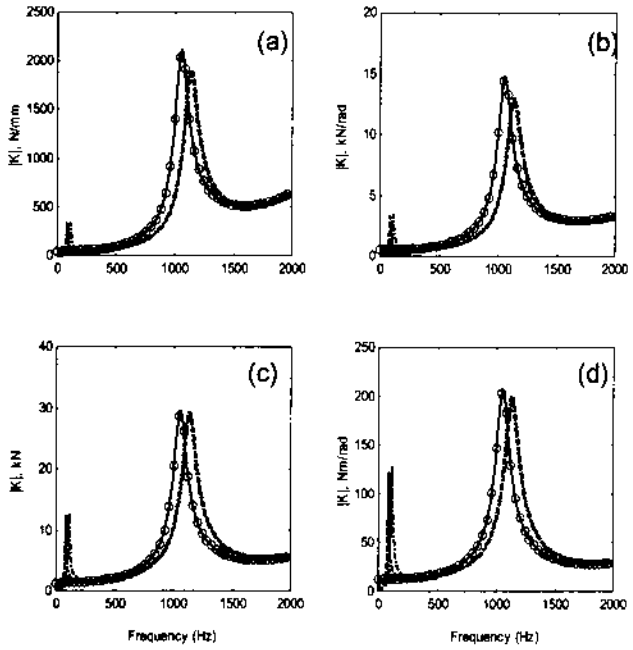

Figure 10. Decomposed flexural stiffnesses for asymmetric beam of Figure 3(d) using a system consisting of two rigid masses and an elastic beam as shown in Figure 3(b). (a) Force stiffness; (b) coupling stiffness; (c) coupling stiffness; (d) moment stiffness. Key: —— , Mobility synthesis method; –·–·– , approximate method using equation (20b); ----- , approximate method using equation (21b); o, direct analytical solution

For the symmetric beam of Figure 3(c), the parameters for the previous section are used again for simulation. For the asymmetric beam case, the beam consists of two sections, as shown in Figure 3(d), of the same E, ρ and η. The radius and length of first section of the beam are 12 mm and 20 mm respectively and the dimensions of the second section of the beam are 24 mm and 20 mm respectively. In simulating these schemes, the system of Figure 3(b) is assumed to be free at both ends. Hence, the additional elastic elements, K_1 and K_2, are not used since this assumption should reduce inaccuracies that may exist in the identification results. As seen in Figure 8(a), the refined identification scheme for axial stiffness based on equation (14) seems to exhibit good results at all frequencies for the symmetric isolator even though the transfer stiffness identified using equation (12) shows discrepancies in the low frequency regime. However, as shown in Figure 8(b), deviations are observed in the asymmetric isolator results, based on both approximate identification schemes. Such deviations come from the approximations made in the identification schemes and the fact that the driving point and the transfer stiffnesses are not equal. In the identification of flexural stiffnesses, discrepancies at low frequencies are observed in either scheme based on (20b) or (21b) for both symmetric and asymmetric isolators as observed in Figures 9 and 10. The refined scheme does not suppress discrepancies at lower frequencies since the effect of difference between driving

point and transfer stiffness matrices still remains imbedded. This is due to the coupling that is introduced by flexural motions. Also, it is seen that deviations are more pronounced for the asymmetric isolator at moderately high frequencies. Nonetheless, it should be noted that the discrepancies beyond the low frequency regime could be reduced when a larger inertial element is used for mass *b*.

IDENTIFICATION OF MOBILITY MATRIX OF AN ISOLATOR

METHODOLOGY: Multi-dimensional mobility matrix of a vibration isolator can be identified using the proposed mobility synthesis formulation. Multi-degree of freedom connections at both ends of an isolator are modeled since information at both ends of a sub-system would be needed. Two masses are attached to an isolator like Figure 3(a) and the synthesized mobility for the overall system is formulated first. Then the mobility matrix of an isolator is reformulated given the synthesized formulation. Finally, the mobility matrix of an isolator can be obtained by substituting the synthesized mobility matrix with measured mobility matrix for the combined system. It is possible to measure all elements of the multi-dimensional mobility matrix from the fact that an application of force with an offset from the reference point results in both force and moment simultaneously.

In order to examine the proposed identification procedure in detail, recall Figure 1(b) that consists of three sub-systems. In this case, we need to identify mobilities $\boldsymbol{\beta}_{ij}$ of component (P). Therefore, mobilities $\mathbf{M}_{ij}$ of the combined system must be measured from specific experiments. The method assumes that $\boldsymbol{\alpha}_{ij}$ and $\boldsymbol{\gamma}_{ij}$ are well known, based on rigid body component theory. Here, i, j = 2,3 for $\boldsymbol{\beta}_{ij}$ and i, j = 1,4 for $\mathbf{M}_{ij}$ and i, j = 1,2 for $\boldsymbol{\alpha}_{ij}$ and i, j = 3, 4 for $\boldsymbol{\gamma}_{ij}$.

For a true three-dimensional motion, mobility matrices $\boldsymbol{\beta}_{ij}$ and $\mathbf{M}_{ij}$ are of dimension 6 and each matrix should be well populated since all motions are interrelated. However, we assume, for the sake of convenience, that each mobility matrix is composed of six diagonal terms and some coupling terms that link linear and angular motions in lateral directions. In other words, we assume that there does not exist any coupling between axial (*x*) and lateral motions (*y* and *z*) with reference to the coordinate system in Figure 1(a). Consequently, the mobility matrix $\boldsymbol{\beta}_{ij}$ of an isolator in three-dimensional motions has the following components:

$$\begin{bmatrix} v_x \\ v_y \\ v_z \\ w_x \\ w_y \\ w_z \end{bmatrix} = \begin{bmatrix} \tilde{M}_{xx}(\omega) & 0 & 0 & \tilde{M}_{x\theta_x}(\omega) & 0 & 0 \\ 0 & \tilde{M}_{yy}(\omega) & \tilde{M}_{yz}(\omega) & 0 & \tilde{M}_{y\theta_y}(\omega) & \tilde{M}_{y\theta_z}(\omega) \\ 0 & \tilde{M}_{zy}(\omega) & \tilde{M}_{zz}(\omega) & 0 & \tilde{M}_{z\theta_y}(\omega) & \tilde{M}_{z\theta_z}(\omega) \\ \tilde{M}_{\theta_x x}(\omega) & 0 & 0 & \tilde{M}_{\theta_x\theta_x}(\omega) & 0 & 0 \\ 0 & \tilde{M}_{\theta_y y}(\omega) & \tilde{M}_{\theta_y z}(\omega) & 0 & \tilde{M}_{\theta_y\theta_y}(\omega) & \tilde{M}_{\theta_y\theta_z}(\omega) \\ 0 & \tilde{M}_{\theta_z y}(\omega) & \tilde{M}_{\theta_z z}(\omega) & 0 & \tilde{M}_{\theta_z\theta_y}(\omega) & \tilde{M}_{\theta_z\theta_z}(\omega) \end{bmatrix} \begin{bmatrix} f_x \\ f_y \\ f_z \\ q_x \\ q_y \\ q_z \end{bmatrix} \quad (22)$$

In this representation, the *x*-axis is the axial direction and the θ_x is the angular motion about the *x*-axis. Hence, coupling terms in these directions vanish.

EXPERIMENTAL STUDIES

EXPERIMENTAL SYSTEM AND MEASURMENT SAMPLES: Mobility model for one rubber isolator (grommets) is identified using the proposed procedure. Two masses are attached to the ends of each isolator and the combined system of Figure 3(a) is suspended to simulate free boundaries. The reciprocity principle has been applied throughout the synthesis procedure since small inconsistencies or noise in frequency response function measurements can significantly contaminate results via the numerical inversion process that is essential to the entire procedure. Figure 11 shows a schematic that is used for experimental work; refer to Table 1 for a listing of instruments. The impulse hammer is used for force excitation and five spectra (up to 2 kHz) are averaged for each measurement. An analog summing circuit is used to decompose the translational accelerations acquired at two opposite locations into rotational motions.

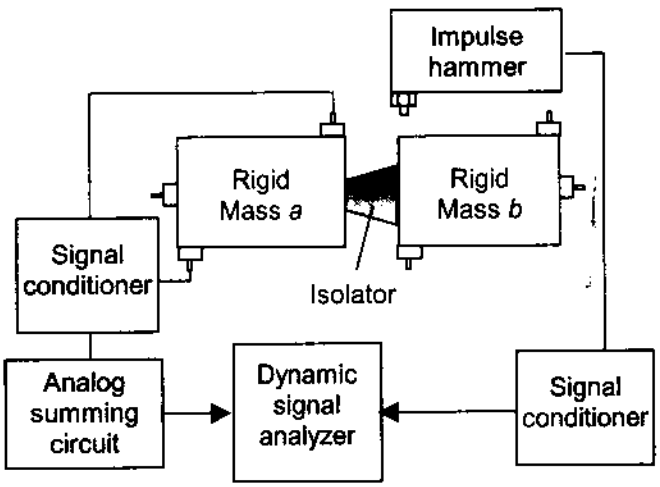

Figure 11. Experimental schematic used to identify mobilities of an isolator.

Table 1. List of instruments used for experimental studies

Item	Manufacturer	Model No.
Accelerometer	PCB	A353B66
Impulse hammer	PCB	086B03
Analog summing circuit	In-house	-
Signal conditioner	PCB	480E09
Dynamic signal analyzer	HP	HP35670A
MTS testing system	MTS	831.50

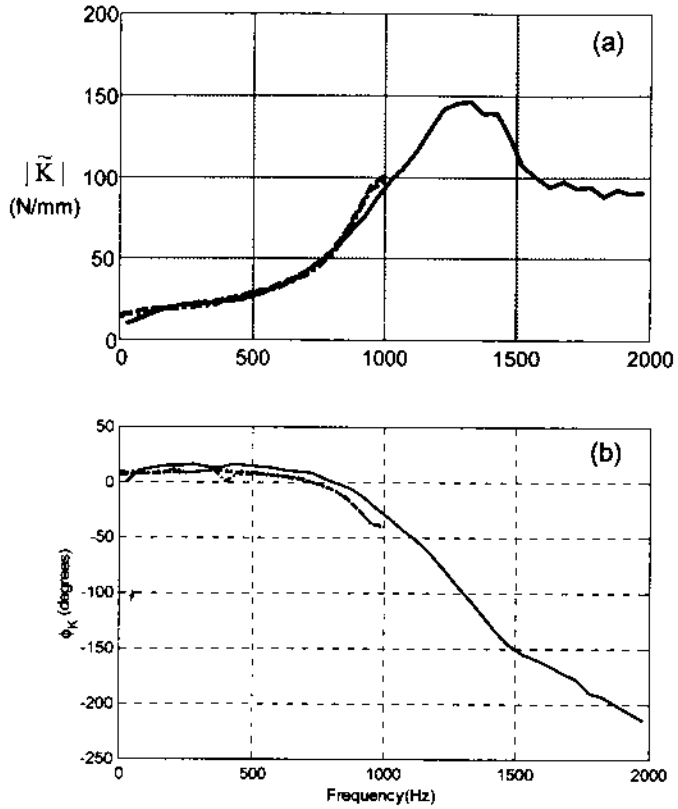

Figure 12. Comparison of axial dynamic stiffnesses for isolator, (a) Dynamic stiffness modulus; (b) loss angle. Key: ——, Mobility model; - - - - -, Measured (MTS): f_{mean} = 3 N; —·—·—, Measured (MTS): f_{mean} = 12 N; ·····, Measured (MTS): f_{mean} = 23 N.

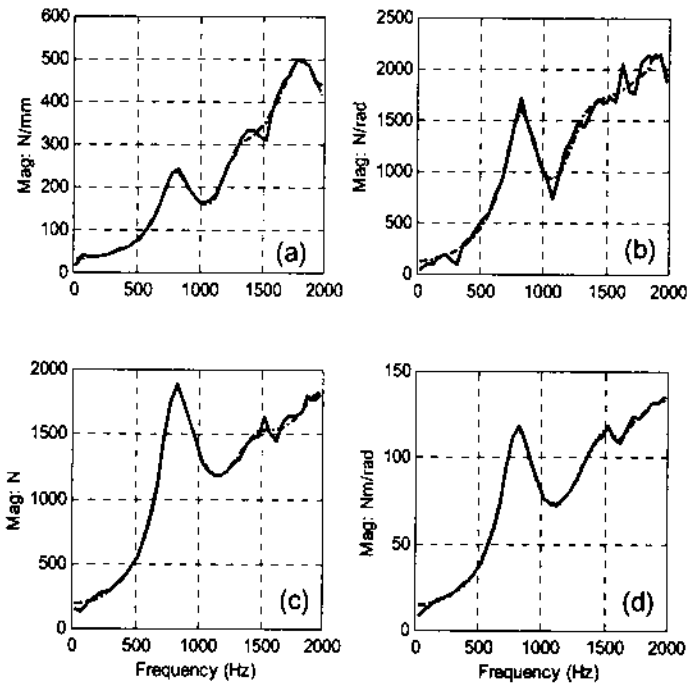

Figure 13. Transfer stiffnesses in flexural motion for isolator, as extracted using the identification scheme. (a) Lateral stiffness modulus; (b) coupling stiffness modulus; (c) coupling stiffness modulus; (d) rotational stiffness. Key: ——, Experimental result; —·—·—, curve fit.

RESULTS AND VALIDATION: Typical results for transfer stiffnesses are shown in Figures 12 and 13 for an isolator example of Figure 2. Note that the experimental validations are conducted using the MTS 831.50 machine (up to 1000 Hz). The MTS method employs the blocked end boundary and only the transfer stiffness is measured. First, stiffness modulus and loss angle in axial direction are shown in Figures 12. Static stiffness in axial motion is 5 N/mm for the isolator. Identified results from the proposed experiment are given from 0 to 2000 Hz. Predictions for zero preload are compared with the MTS test results that are obtained under three different preloads, up to 1 kHz. Excellent agreements are observed between results based on the proposed identification method and experimental data yield by the MTS machine. Similar results are seen for two additional mounts [15].

CONCLUSION

A new characterization method has been proposed for the identification of multi-dimensional frequency-dependent transfer stiffnesses of an isolator. Our method uses a physical system that consists of two inertial elements and an isolator. Further, refined multi-dimensional mobility synthesis and decomposition procedures have been formulated. Results of the proposed scheme compare well with test data for one practical isolator in axial motions on a commercial machine up to 1 kHz. Also, approximate identification methods, as proposed by Thompson et. al. [12], are critically analyzed for axial stiffnesses. Aforementioned method [12] is then extended to the identification of isolator stiffnesses in flexure. One simulation example is carried out for both symmetric and asymmetric isolators. Such approximate methods show some discrepancies from the exact stiffness in low and moderately high frequency regimes, depending upon the isolator, due to the simplifications that are made in the formulation of such methods. For instance, this disagreement is pronounced for an asymmetric isolator. Further work is required to fully understand this and other research issues.

ACKNOWLEDGMENTS

The General Motors Corporation (Noise and Vibration Center) and the Goodyear Tire and Rubber Company (Transportation Molded Products) are gratefully acknowledged for supporting this research.

REFERENCES

1. C. M. HARRIS 1987 *Shock and Vibration handbook*. New York: McGraw-Hill Book Company.
2. J. C. SNOWDON 1968 *Vibration and Shock in Damped Mechanical Systems*. New York: John Wiley & Sons, Inc.
3. J. I. SOLIMAN and M. G. HALLAM 1968 *Journal of Sound and Vibration*, **8**(2), 329-351. Vibration Isolation between Non-Rigid Machines and Non-Rigid Foundations.

4. H. G. D. GOYDER and R. G. WHITE 1980 *Journal of Sound and Vibration*, **68**(1), 97-117. Vibrational Power Flow from Machines into Built-Up Structures, Part III: Power Flow Through Isolation Systems.
5. L. F. NIELSEN, N. J. WISMER and S. GADE 2000 *Sound and Vibration,* February, 20-24. An Improved Method for Estimating the Dynamic Properties of Materials
6. T. JEONG 2000 *Ph.D. Thesis, The Ohio State University*, Analysis of Powertrain Mounts with Focus on Torque Roll Axis Decoupling and Frequency-dependent Properties.
7. M. A. SANDERSON 1996 *Journal of Sound and Vibration*, **198**(2), 171-191. Vibration Isolation: Moments and Rotations Included.
8. S. NADEAU and Y. CHAMPOUX 2000 *Experimental Techniques*, May/June, 21-23. Application of the Direct Complex Stiffness Method to Engine Mounts.
9. MTS Systems Corporation 1999 *User Manual.*
10. D. J. THOMPSON and N. VINCENT 1995 *Vehicle System Dynamics Supplement*, **24**, 86-99. Track dynamic behavior of at High Frequencies. Part 1: Theoretical Models and Laboratory Measurements.
11. D. J. THOMPSON and J. W. VERHEIJ 1997 *Applied Acoustics*, **52**, 1-17. The Dynamic Behavior of Rail Fasteners at High Frequencies.
12. D. J. THOMPSON, W. J. VAN VLIET and J. W. VERHEIJ 1998 *Journal of Sound and Vibration*, **213**(1), 169-188. Development of the Indirect Method for Measuring the High Frequency Dynamic Stiffness of Resilient Isolator.
13. Å. FENANDER 1997 *Journal of Rail and Rapid Transit, Proceedings of I.Mech.E. Part F*, **211**, 51-62. Frequency Dependent Stiffness and Damping of Railpads.
14. C. M. RICHARDS and R. SINGH 2000 *submitted to the Journal of Sound and Vibration*, Experimental Characterization of Rubber Isolator Nonlinearities in the Context of Single and Multi-Degree-of-Freedom Vibratory Systems.
15. S. KIM and R. SINGH 2000 *Journal of Sound and Vibration*, Multi-Dimensional Characterization of Vibration Isolators over a Wide Range of Frequencies (in press).

LIST OF SYMBOLS

d	diameter
E	Young's modulus
f	force amplitude
$\mathbf{f}$	force amplitude vector
$\mathbf{F}$	excitation vector
h	reference location in rigid body with respect to mass center
$\mathbf{I}$	identity matrix
I_S	area moment of inertia
I_m	mass moment of inertia
j	$\sqrt{-1}$
K	stiffness
$\mathbf{K}$	stiffness matrix
L	length
m	mass
$\mathbf{m}$	inertia matrix
M	mobility
$\mathbf{M}$	mobility matrix
q	moment amplitude
$\mathbf{q}$	moment amplitude vector
$\mathbf{R}$	rotation matrix for the cross vector product
S	section area
S, P, R	source, path and receiver
$\mathbf{T}$	transformation matrix
X	displacement in x direction
Y	displacement in y direction
v	translational velocity
$\mathbf{v}$	translational velocity vector
$\mathbf{V}$	velocity vector
w	rotational velocity
$\mathbf{w}$	rotational velocity vector
x, y, z	cartesian coordinates
α, β, γ	mobilities of components
$\boldsymbol{\alpha}, \boldsymbol{\beta}, \boldsymbol{\gamma}$	mobility matrices of components
η	loss factor
θ	rotational displacement
ρ	density
ω	frequency, rad/sec

Subscripts

G	mass center
a, b	mass a and b
B	flexural motion
i, j	indices or reference points in mass
L	axial or longitudinal motion
mean	mean load
S, P, R	source, path and receiver
v	translational component of mobility matrix of rigid body
w	rotational component of mobility matrix of rigid body
x, y, z	cartesian coordinates
1, 2, 3, 4	reference locations

Superscripts

T	transpose
~	complex valued
', "	frequency used for criterion

Operators

Δ	determinant of system matrix
diag	diagonal matrix
|	complex quotient operation for matrices